

Biophysical Journal, Volume 97

Supporting Material

**Protein-Induced Membrane Curvature Investigated Through Molecular Dynamics
Flexible Fitting**

Jen Hsin, James Gumbart, Leonardo G. Trabuco, Elizabeth Villa, Pu Qian, C. Neil
Hunter, and Klaus Schulten

Supporting Materials

Movies

MovieS1 The trajectory of the membrane-reshaping process in Sim1. Water and ion molecules were not included.

MovieS2 The trajectory of the membrane-reshaping process in Sim2. Water and ion molecules were not included.

MovieS3 An animation of the best-fit surfaces of the membrane patch in Sim1, obtained using the shape-fitting protocol (see Method). At the end of the animation, the best-fit surface of the last frame is colored by r_x , with the color scale shown in Fig. 5A.

MovieS4 An animation of the best-fit surfaces of the membrane patch in Sim2, obtained using the shape-fitting protocol (see Method). At the end of the animation, the best-fit surface of the last frame is colored by r_x , with the color scale shown in Fig. 5B.

Additional figures

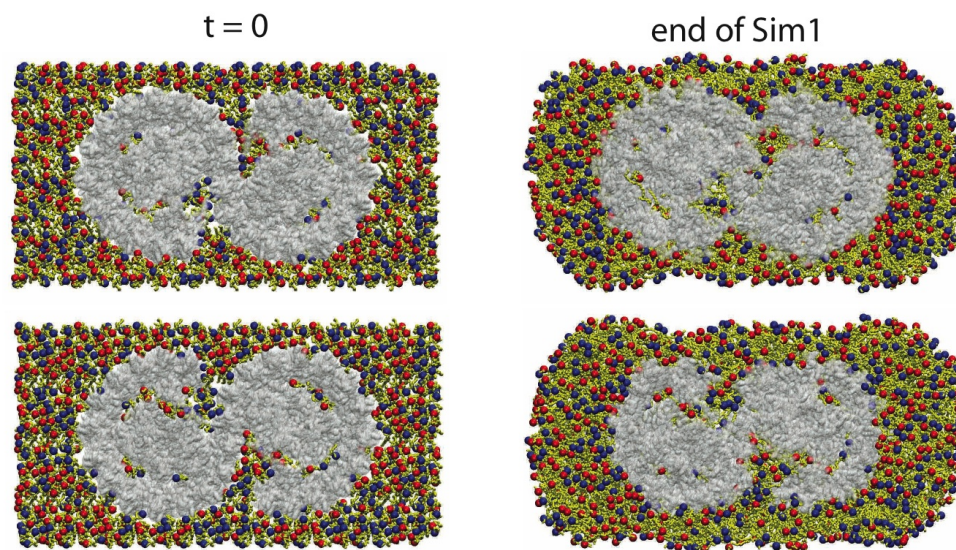


Figure S1: Distribution of lipid types in the 50% POPE/50% POPG membrane patch used in the reported simulations. Shown here are snapshots of the system before the simulations and after Sim1 (Sim2 uses the same membrane patch) for both top and bottom views. The RC-LH1-PufX dimer is shown as a gray surface; lipid molecules are shown in yellow, with the phosphorus atoms shown as blue and red spheres for the POPE and POPG phosphorus atoms, respectively.

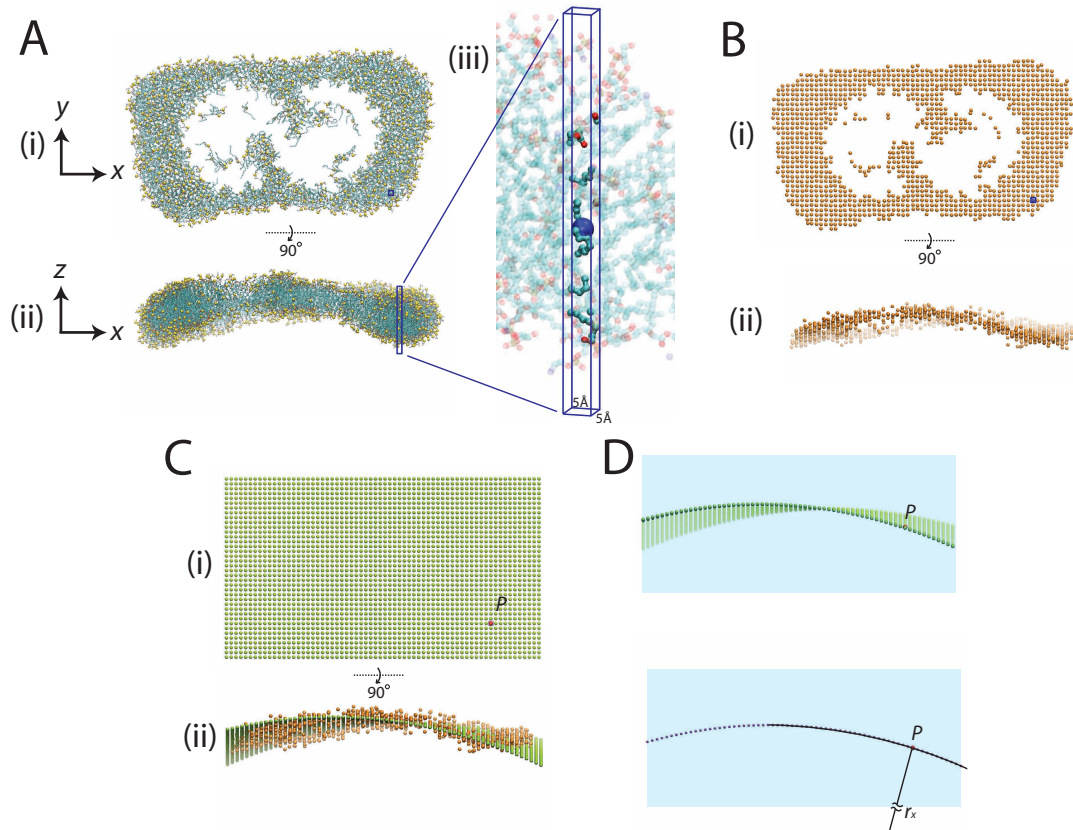


Figure S2: Membrane curvature analysis protocol. (A) A membrane patch was first divided into 5 \AA by 5 \AA vertical square prisms, and the positions of lipid heavy atoms in each square prism were averaged. (A-iii) shows an example square prism and the lipid atoms within; the blue sphere represents the averaged lipid position within this square prism. (B) Average shape of the membrane patch. (C) Best-fit surface (colored in green), in the form of Eq. 2, computed for the average shape of the membrane patch (colored in orange). (D) Calculation of the radius of curvature. For a point P on the surface, the radius of curvature along the x -axis, r_x , is computed by measuring the radius of the osculating circle passing point P that lies in the x - z plane.

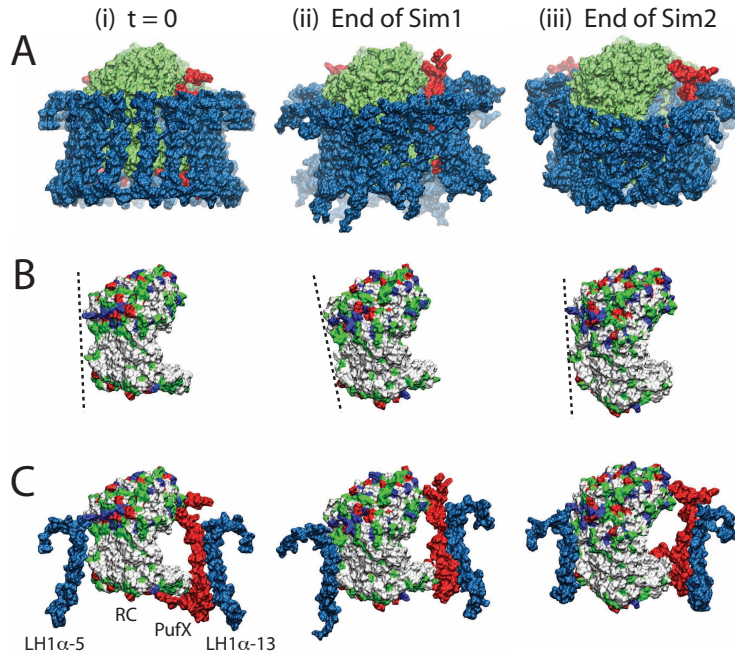


Figure S3: Twisting of the membrane is correlated with the RC orientation within the RC-LH1-PufX dimer. (A) Side view of the protein along the long dimer axis (i) at $t = 0$, (ii) at the end of Sim1, and (iii) at the end of Sim2. The RC is shown in green, PufX in red, and LH1 α in blue; LH1 β is not shown for clarity. At $t = 0$, the system is symmetric. At the end of Sim1, the two LH1 monomers swung in opposite directions. For Sim2, the dimer stayed symmetric when confined within the EM map. In (B), LH1 and PufX are not shown, and only the RC closer to the view is shown for clarity, colored according to residue type: non-polar residues in white, polar residues in green, positively charged residues in blue, and negatively charged residues in red. (C) RC and its neighboring LH1 α (LH1 α -5 and LH1 α -13, colored in blue) and PufX (colored in red). By the end of Sim1, LH1 α and PufX became closely associated with the RC, and tilting in RC occurred similar to the tilting in the LH1 and PufX helices. In Sim2, RC, LH1 and PufX remained vertical.

Structural features of the bent RC-LH1-PufX dimer model

The MDFF simulation, followed by a 29-ns equilibration in Sim1, provided an atomic model for the bent RC-LH1-PufX dimer. One should, however, be cautious in interpreting structural information through this model. In particular, the extrinsic regions of the RC-LH1-PufX dimer are not well-resolved in the EM map of the negatively stained dimers (1) and, therefore, during the MDFF simulations, the C- and N-termini of LH1 and PufX are likely distorted through artificial steering into the density map. The long equilibration following MDFF possibly remedied this problem by allowing the LH1 and PufX extrinsic regions to search for their natural positions, but the accuracy of the final model cannot ultimately be determined without a high-resolution structure. An issue in this regard is the actual location of PufX. Here, we discuss features of the bent RC-LH1-PufX dimer model resulting from Sim1 and how they reflect upon the known structural and functional properties of RC-LH1-PufX. The discussion here focuses on structural aspects of the RC-LH1-

PufX protein; the pigment organization within the RC-LH1-PufX dimer resulted from the MDFF simulations is discussed in Şener et al. (2).

A key observation of the RC-LH1-PufX model obtained through Sim1 is the high surface complementarity seen at the RC-LH1 and LH1-PufX interfaces, illustrating close hydrophobic interactions (Fig. S4). PufX is found tightly associated with the neighboring LH1 α helices (LH1 α -13 and LH1 α -14 for one RC-LH1-PufX monomer and LH1 α -27 and LH1 α -28 for the other monomer; the numbering of LH1 helices is shown in Fig. 1A), in agreement with a reconstitution study suggesting interactions between LH1 α and PufX (3). Surface complementarity can be quantitatively described by measuring the contact surface area between two proteins. The contact surface area was measured to be approximately 700 Å² between PufX and LH1 α -13 after Sim1 (compared to 500 Å² at $t = 0$), and 550 Å² between PufX and LH1 α -14 (compared to 330 Å² at $t = 0$; see also Table S1). To get a sense of what contact surface area implies close interaction, we note that each pair of α/β -apoproteins in *Phaeospirillum molischianum* (renamed from *Rhodospirillum molischianum* (4)) LH2 has approximately 620 Å² of contact surface area, and the neighboring α -apoproteins have 550 Å² contact surface area (5). By comparing with the LH2 helices, one can conclude that PufX is closely associated with the LH1 α -13 and LH1 α -14 helices, in agreement with previous experimental studies (3, 6). It is also worth noting that a salt bridge between LH1 β -13 Asp5 and PufX Arg20 formed at the end of Sim1 (Fig. S4A-iii), enhancing the PufX-LH1 association in addition to the hydrophobic interaction with LH1 α . In total, it was observed that PufX interacts most closely with LH1 α , and less so with LH1 β or RC. This permits PufX to dock, in principle, at any location where LH1 α is available.

	$t = 0$	after Sim1
PufX/LH1 α -13	500	700
PufX/LH1 α -14	330	550
RC/LH1 α -4	150	840
RC/LH1 α -5	270	570

from crystal structure	
LH2 α/β	620
LH2 α/α	550

Table S1: Contact surface area (in Å²) characterizing the PufX-LH1 and RC-LH1 associations. The LH2 α/β and LH2 α/α (between neighboring α helices) contact surface areas were also measured for comparison, using the LH2 structure from *Phaeospirillum molischianum* (PDB entry 1LGH) (5).

High surface complementarity was also found between the RC and its neighboring LH1 α helices.

Fig. S4B shows that the shape of the RC surface matches that of LH1 α -4 and LH1 α -5. The contact surface area was measured to be 840 Å² between RC and LH1 α -4, and 570 Å² between RC and LH1 α -5 (see also Table S1). Moreover, a network of salt bridges between LH1 and the RC was found (Fig. S5). Fig. S5A shows the four salt bridges formed by the end of Sim1 in one of the RC-LH1-PufX monomers (LH1 β -15 Lys3:RC-H Asp46, LH1 β -19 Asp2:RC-L Lys202, LH1 α -17 Arg15:RC-H Glu94, and LH1 α -19 Asp12:RC-H Lys60). All of the residues participating in salt bridges are located outside of the membrane in the flexible loop/coil region. The location of these residues has two likely advantages: during RC-LH1-PufX formation, the flexibility of the loop/coil region allows for wider motions of these residues, permitting them to search for other salt bridge partners; after the dimer is formed, the network of salt bridges ensures structural integrity of the dimer, while the flexibility of their locations allows for the dimer’s internal flexibility, essential for the function of the protein. Indeed, the photosynthesis process requires migration of quinone/quinol molecules into and out of the RC. It is still not well understood how the quinone/quinol molecules pass through the LH1 ring (7); it has been suggested that LH1 exhibits “breathing” motions that facilitate the passage of quinone/quinol (8–11). Flexibility of LH1 is also supported by atomic force microscopy images showing a wide variation in the shape of LH1 in *Rba. sphaeroides* mutants lacking LH2 and RC (12), as well as the observation of both elliptical and circular RC-LH1 rings in *Rsp. rubrum* (8, 9).

Another source of RC-LH1-PufX dimer flexibility is the availability of multiple salt bridge partners for the RC residues, shown in Fig. S5B. At the beginning of the simulation, Lys60 of RC-H formed a salt bridge with Asp12 of LH1 α -5. During equilibration, this salt bridge was broken and Lys60 of RC-H formed a salt bridge with Asp5 of LH1 β -4 instead. Having such “back-up” salt bridges provides conformational freedom for the LH1 helices around the RC without losing the LH1-RC association. The RC residues identified to participate in salt bridges with LH1 are RC-H Asp46, RC-L Lys202, RC-H Glu94, and RC-H Lys60. Mutation of these residues into neutral alternatives should weaken the RC-LH1 association and may even inhibit the formation of the RC-LH1 complex.

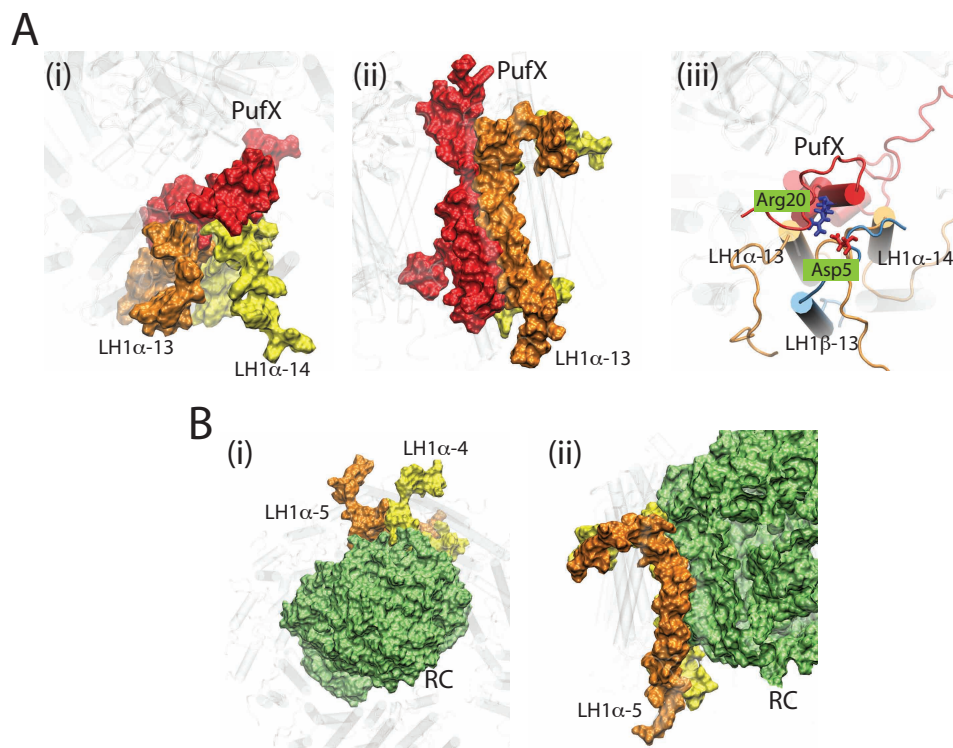


Figure S4: PufX-LH1 and RC-LH1 association. Surface complementarity was observed between the PufX-LH1 interface, shown here in a top view perpendicular to the membrane plane (A-i) and a side view along the dimer long axis (A-ii). PufX, LH1 β -13 and β -14 are displayed in surface representation; PufX colored in red, LH1 α -14 in yellow and LH1 α -13 in orange. (A-iii) Salt bridge formed at the end of Sim1 between PufX Arg20 and LH1 β -13 Asp5. PufX and LH1 are displayed in cartoon representation, with PufX in red, LH1 α in orange, and LH1 β in blue. Residues forming salt bridges are highlighted in licorice representation and colored according to residue type (blue for positive residues and red for negative residues). (B) Surface complementarity between the RC-LH1 interface, shown from the top (B-i) and from the side (B-ii). RC, LH1 α -4 and LH1 α -5 are shown in surface representation; RC colored in green, LH1 α -4 in yellow, and LH1 α -5 in orange.

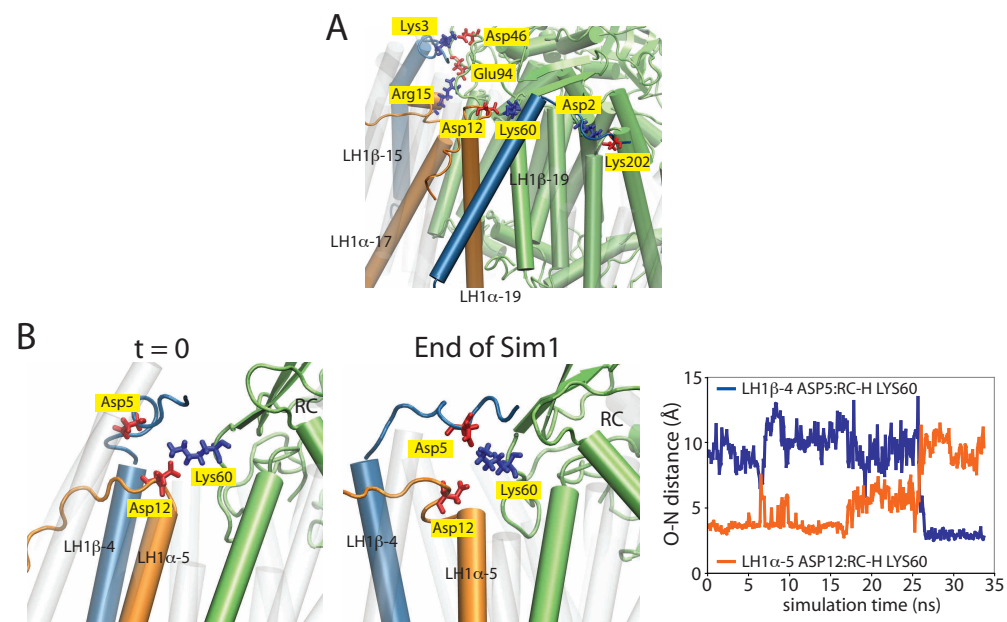


Figure S5: Network of salt bridges between LH1 and RC. In (A), four salt bridges are shown in one of the RC-LH monomers (LH1 β -15 Lys3:RC-H Asp46, LH1 β -19 Asp2:RC-L Lys202, LH1 α -17 Arg15:RC-H Glu94, and LH1 α -19 Asp12:RC-H Lys60). The RC is shown in green, LH1 α in orange, and LH1 β in blue. Residues forming salt bridges are highlighted in licorice representation and colored according to residue type (blue for positive residues and red for negative residues). (B) Example of a "back-up" salt bridge. At the beginning of the simulation, RC-H Lys60 formed a salt bridge with LH1 α -5 Asp12; during the equilibration, this salt bridge became broken and RC-H Lys60 formed a salt bridge with LH1 β -4 Asp5 instead.

References

1. Qian, P., P. A. Bullough, and C. N. Hunter. 2008. Three-dimensional reconstruction of a membrane-bending complex: The RC-LH1-PufX core dimer of *Rhodobacter sphaeroides*. *J. Biol. Chem.* 283:14002–14011.
2. Sener, M. K., J. Hsin, L. G. Trabuco, E. Villa, P. Qian, C. N. Hunter, and K. Schulten. 2009. Structural model and excitonic properties of the dimeric RC-LH1-PufX complex from *Rhodobacter sphaeroides*. *Chem. Phys.* 357:188–197.
3. Tunncliffe, R. B., E. C. Ratcliffe, C. N. Hunter, and M. P. Williamson. 2006. The solution structure of the PufX polypeptide from *Rhodobacter sphaeroides*. *FEBS Lett.* 580:6967–6971.
4. Imhoff, J. F., R. Petri, and J. Süling. 1998. Reclassification of species of the spiral-shaped phototrophic purple non-sulfur bacteria of the alpha-proteobacteria: description of the new genera *Phaeospirillum* gen. nov., *Rhodovibrio* gen. nov., *Rhodothalassium* gen. nov. and *Roseospira* gen. nov. as well as transfer of *Rhodospirillum fulvum* to *Phaeospirillum fulvum* comb. nov., of *Rhodospirillum molischianum* to *Phaeospirillum molischianum* comb. nov., of *Rhodospirillum salinarum* to *Rhodovibrio salexigens*. *Int. J. Syst. Bacteriol.* 48:793–798.
5. Koepke, J., X. Hu, C. Muenke, K. Schulten, and H. Michel. 1996. The crystal structure of the light harvesting complex II (B800-850) from *Rhodospirillum molischianum*. *Structure.* 4:581–597.
6. Recchia, P., C. Davis, T. Lilburn, J. Beatty, P. Parkes-Loach, C. Hunter, and P. Loach. 1998. Isolation of the PufX protein from *Rhodobacter capsulatus* and *Rhodobacter sphaeroides*: evidence for its interaction with the α -polypeptide of the core light-harvesting complex. *Biochem.* 37:11055–11063.
7. Blankenship, R. E. 2002. *Molecular Mechanisms of Photosynthesis*. Blackwell Science, Malden, MA.
8. Jamieson, S. J., P. Wang, P. Qian, J. Y. Kirkland, M. J. Conroy, C. N. Hunter, and P. A. Bullough. 2002. Projection structure of the photosynthetic reaction centre-antenna complex of *Rhodospirillum rubrum* at 8.5 Å resolution. *J. Mol. Biol.* 21:3927–3935.
9. Fotiadis, D., P. Qian, A. Philippsen, P. A. Bullough, A. Engel, and C. N. Hunter. 2004. Structural analysis of the reaction center light-harvesting complex I photosynthetic core complex of *Rhodospirillum rubrum* using atomic force microscopy. *J. Biol. Chem.* 279:2063–2068.
10. Bahatyrova, S., R. N. Frese, C. A. Siebert, J. D. Olsen, K. O. van der Werf, R. van Grondelle, R. A. Niederman, P. A. Bullough, C. Otto, and C. N. Hunter. 2004. The native architecture of a photosynthetic membrane. *Nature.* 430:1058–1062.

11. Aird, A., J. Wrachtrup, K. Schulten, and C. Tietz. 2007. Possible pathway for ubiquinone shuttling in *R. rubrum* revealed by molecular dynamics simulation. *Biophys. J.* 92:23–33.
12. Bahatyrova, S., R. N. Frese, K. O. van der Werf, C. Otto, C. N. Hunter, and J. D. Olsen. 2004. Flexibility and size heterogeneity of the LH1 light harvesting complex revealed by atomic force microscopy. *J. Biol. Chem.* 279:21327–21333.